Published in final edited form as:
Neuron. 2008 June 26; 58(6): 884–896.

DAG Lipase Activity Is Necessary for TRP Channel Regulation in Drosophila Photoreceptors

Hung-Tat Leung[1], **Julie Tseng-Crank**[1,3,*], **Eunju Kim**[1,*], **Cecon Mahapatra**[1], **Shikoh Shino**[1], **Ying Zhou**[1,4], **Lingling An**[2], **Rebecca W. Doerge**[2], and **William L. Pak**[1,†]

1 *Department of Biological Sciences, Purdue University*

2 *Department of Statistics, Purdue University*

3 *Now at Unigen Pharmaceuticals, Lacey, WA 98516*

4 *Now at Department of Biology, University of Massachusetts Amherst*

Summary

In *Drosophila*, a phospholipase C-mediated signaling cascade links photo-excitation of rhodopsin to the opening of the TRP/TRPL channels. A lipid product of the cascade, DAG (diacylglycerol) and its metabolite(s), polyunsaturated fatty acids (PUFAs), have both been proposed as potential excitatory messengers. A crucial enzyme in the understanding of this process is likely to be DAG lipase (DAGL). However, DAGLs which might fulfill this role have not been previously identified in any organism. In this work, the *Drosophila* DAGL gene, *inaE*, has been identified from mutants that are defective in photoreceptor responses to light. The *inaE*-encoded protein isoforms show high sequence similarity to known mammalian DAG lipases, exhibit DAG lipase activity *in vitro*, and are highly expressed in photoreceptors. Analyses of *norpA inaE* double mutants and severe *inaE* mutants show that normal DAGL activity is required for the generation of physiologically meaningful photoreceptor responses.

Introduction

Visual transduction in *Drosophila* utilizes a G-protein-coupled, phospholipase C-mediated signaling cascade. Phospholipase C, upon activation via rhodopsin and G-protein, Gq, catalyzes the hydrolysis of phosphatidylinositol 4,5-bisphosphate (PIP_2) into two potential second messengers, diacylglycerol (DAG) and inositol trisphosphate (IP_3). A body of evidence suggests that IP_3 is not involved in *Drosophila* phototransduction (Acharya et al., 1997; Raghu et al., 2000), leaving the DAG branch as a likely source of messenger(s) of activation for the phototransduction channels, TRP (*transient receptor potential*) and TRPL (TRP-like). The mechanism by which the diacylglycerol (DAG) branch might activate the TRP/TRPL channels is still unresolved. The first indication that a lipid messenger might be involved was provided by Chyb et al. (1999), who showed that polyunsaturated fatty acids (PUFAs) could activate both TRP and TRPL channels either in intact photoreceptors or heterologous expression systems. Later, the same group presented evidence that DAG is required for photoreceptor excitation using DAG kinase mutants, *rdgA* (Masai et al., 1993). Because the conversion of DAG to phosphatidic acid is blocked in these mutants, they should have an elevated DAG basal level. These investigators showed that TRP/TRPL channels are constitutively active in *rdgA* (Raghu et al., 2000) and that diminished responses of hypomorphic PLC (*norpA*) mutants could be greatly enhanced by *rdgA* mutations (Hardie et al., 2002), in support of the contention that

†Corresponding author: William L. Pak.
*Contributed equally to this work

DAG might be excitatory to the channels. However, *rdgA* mutations are expected to raise the basal levels of not only DAG but also its metabolites. In addition to these two molecules, phosphatidylinositol 4,5-bisphosphate (PIP_2) has also been suggested to play a role in channel excitation (review: Hardie, 2002). Currently, no consensus exists as to which, if any, of these might be the excitatory agent for TRP/TRPL channels.

Drosophila TRP is the founding member of a superfamily of TRP channel proteins. There are now nearly 30 mammalian members of this superfamily comprising seven subfamilies (reviews: Montell, 2005; Minke, 2006; Hardie, 2007). Although these channels are heterogeneous in their modes of activation, at least four mammalian TRP channels have been reported to be activated by DAG: TRPC2, 3, 6, and 7. While there may be variations in the mechanisms of activation of these channels, elucidation of *Drosophila* TRP/TRPL channel activation could provide insight into activation of these channels as well.

Since both DAG and its potential metabolite, PUFA, have been implicated in the activation of TRP/TRPL channels, a key enzyme in this process is likely to be DAG lipase, which catalyzes the hydrolysis of DAG. Little is known about DAG lipases. Two mammalian DAG lipase genes, DAGLα and β, have been identified by a bioinformatics approach and characterized both biochemically and molecularly (Bisogno et al., 2003), and many proteins homologous to DAGα and β have been identified across species. In the case of *Drosophila*, Huang et al. (2004) have described a mutant, *rolling blackout (rbo*), which they suggested might be in a DAG lipase gene. The protein encoded by the *rbo* gene, however, shows little homology to the known mammalian DAG lipases. Moreover, conditional loss of the RBO protein leads to rapid depletion of DAG, the opposite of what one would expect if RBO catalyzes the hydrolysis of DAG. Furthermore, in the absence of previous activity, the receptor potential is normal in *rbo* mutants, making it unlikely that RBO has any direct involvement in the activation of TRP/TRPL channels (Huang et al., 2004). Other than *rbo*, no candidate DAG lipase that might function in phototransduction has been reported in any species.

In this work, we report on a *Drosophila* DAG lipase (DAGL) gene, *inaE*, identified from mutants that are defective in photoreceptor responses to light. The protein isoforms encoded by this gene show high sequence similarity to the two known mammalian DAGLs, exhibit DAGL activity *in vitro*, are highly expressed in photoreceptors, and have access to rhabdomeres. Genetic evidence suggests that the *inaE*-encoded DAGLs interact *in vivo* with the DAG generated in the phototransduction cascade. Analysis of mutants generated by imprecise excision of P-element insertion in *inaE*, show that no physiologically meaningful photoreceptor responses can be generated if *inaE* gene is severely impaired.

Results

Mutant ERG phenotypes

The *inaE* gene was identified by two EMS (ethylmethane sulfonate)-induced allelic mutants, *N125* and *P19*. These mutants are characterized by their "*ina*" (inactivation, no afterpotential) ERG (electroretinogram) phenotype. Wild-type flies, when placed on a white-eye (*w*) background, respond to a bright blue stimulus with a large response during light stimulus followed by a prolonged depolarizing afterpotential (PDA) after the light is turned off (Fig. 1A). A second blue stimulus elicits only a small response, originating from R7/8 photoreceptors, superposed on the PDA. By contrast, in *ina* mutants, the response begins to decay during stimulus (inactivation; arrowhead, Fig. 1A), and the decay continues after the stimulus (arrow, Fig. 1A). As a result, the PDA is greatly diminished in amplitude (no afterpotential). This phenotype can also be viewed as a mild form of the "*trp*" phenotype displayed by strong mutants of the TRP channel gene. As illustrated in Fig. 1A, in *trp* mutants,

the response to the first blue stimulus decays nearly to baseline during stimulus, and there is no PDA.

Moreover, responses of *inaE* mutants resemble those of *trp* in that they both display refractory properties. Following a response to the first stimulus, only very small responses can be elicited from *trp* until they recover over a period of minutes (Fig. 1B, bottom traces), while wild-type responses recover almost immediately (Fig. 1B, top traces). Likewise, *inaE* mutants exhibit a similar refractory period, although the degree and duration of response suppression are not as pronounced or prolonged as in *trp* (Fig. 1B, middle traces).

In addition to the above similarities, $inaE^{N125}$ acts as a genetic enhancer of Trp^{P365}. Trp^{P365} is a semidominant allele of *trp*, which causes constitutive activation of TRP channels and, as a result, massive photoreceptor degeneration from excessive Ca^{2+} influx (Yoon et al., 2000). In Trp^{P365} homozygotes, degeneration is already so advanced in 1–2 d-old flies that essentially no ERGs can be elicited (Fig. 1C-a, top trace). Trp^{P365} heterozygotes exhibit a much milder phenotype and elicit ERGs of substantial amplitude at the same age (Fig. 1C-a, middle trace). However, if $inaE^{N125}$ is introduced into the Trp^{P365}/+ background, the resulting phenotype is as severe as that of Trp^{P365} homozygotes (Fig. 1C-b). The genetic enhancement of Trp^{P365}/+ by $inaE^{N125}$ and the basic similarity of ERG phenotypes between *inaE* and *trp* mutants (Fig. 1A–B) led to the hypothesis that the protein products of these two genes may interact and/or subserve closely related functions.

inaE cloning

A. Identification of an *inaE* candidate gene—Although we initially attempted traditional positional cloning approaches, the approach that ultimately proved successful was one based on DNA microarrays (review: Leung et al., 2007). Mutations that affect the ERG almost always also affect the level of mRNA produced by the mutated genes. Accordingly, DNA microarrays were carried out on $inaE^{N125}$ and its corresponding wild type to look for genes that are altered in mRNA levels within the mapped limit of the mutant.

Deficiency mapping placed the *inaE* gene within the cytogenetic interval 12C5-6 to 12C8-D1 on the X chromosome. The deficiencies that were critical for this mapping were $Df(1)ben^{CO2}$ (12C5-6;12E) and *Df(1)AR10* (12B1-2;12C8-D1), which both uncovered *inaE* (Fig. 2A). To be conservative, we examined microarray data from a much larger region than that determined by mapping, 12B4 to 12D4, a ca. 350 kb region with 41 genes. Within this interval, the following three genes exhibited the greatest and/or statistically most significant changes in mRNA level in $inaE^{N125}$ compared to wild type: *Yp3* at 12C1, *CG33174* at 12C4-5, and *CG32626* at 12C6-7 (Fig. 2B). The only RNA changes to which statistical analysis assigned a p-value of 0 in this interval were those corresponding to *CG33174*. Complementation tests between $inaE^{N125}$ and the existing *Yp3* mutants ruled out *Yp3* as a candidate gene. Southern blots of deficiency heterozygotes probed with DNA fragments from *CG32626* showed that this gene is outside the mapped limits of *inaE*, leaving *CG33174* as the only viable candidate for *inaE*.

B. Validation of candidate gene identification—To verify the identification, we carried out the following series of validation experiments. 1) Sequencing: Sequencing the *CG33174* gene in $inaE^{N125}$ showed that $inaE^{N125}$ carries a G->A transition at the 5′ splice site of the 11^{th} intron (Fig. 2B). 2) P-insertion lines: We obtained four P element-insertion lines in this gene listed in Flybase. None of these showed any obvious ERG phenotype. However, one of them, *KG08585*, which carries a P insertion just outside the 13^{th} exon (Fig. 2B), mimicked $inaE^{N125}$ in enhancing the Trp^{P365}/+ phenotype, when introduced into the Trp^{P365}/+ background in a homoallelic combination (*KG08585/KG08585;* Trp^{P365}/+) (Fig. 1C-c). More importantly, *KG08585* in a heteroallelic combination with $inaE^{N125}$ also enhanced the

Trp^{P365}/+ phenotype (*KG08585*/$inaE^{N125}$; Trp^{P365}/+) (Fig. 1C-c). Thus, *KG08585* failed to complement $inaE^{N125}$. 3) *In vivo* rescue: The *CG33174* gene is predicted to encode two protein isoforms, PA and PD, through alternative splicing (Fig. 2B). We made cDNA rescue constructs of both the D and A forms, driven by the *trp* promoter. The D construct, but not the A construct, when introduced into the $inaE^{N125}$ background by germline transformation, rescued the mutant ERG phenotype (Fig. 1D). Moreover, in the presence of the construct, $inaE^{N125}$ no longer enhanced the Trp^{P365}/+ phenotype (Fig. 1C-d). The A construct, on the other hand, did not have this effect (Fig. 1C-e). The above three lines of evidence unequivocally established *CG33174* as the *inaE* gene.

Identification of the INAE proteins as diacylglycerol lipases

The *CG33174* gene had not been characterized previously, and its function was electronically inferred as “triacylglycerol lipase (TAGL) activity” (Flybase). However, we considered the possibility that the above annotation could simply reflect dearth of information on DAGLs. The first two human DAGLs, DAGLα and β, were cloned and characterized by Bisogno, et al. (2003) by a bioinformatic approach and shown to be *sn-1* type DAGLs. Multiple alignment of INAE-A and INAE-D with DAGLα and β revealed extensive sequence and domain conservations (Fig. 1, Supplemental Material). All four proteins are predicted to have four transmembrane segments near the N-terminal region, and they all have a lipase_3 domain with a highly conserved serine active site (Fig. 1, Supplemental Material). Overall sequence homology between INAE-D and the two human DAGLs is 39% identity and 56% similarity for DAGLα and 30% identity and 50% similarity for DAGLβ, respectively. In the lipase_3 domain, the sequence homology between INAE-A/D and the mammalian proteins rises to 60% and 45% identity and 73% and 63% similarity for DAGLα and DAGLβ, respectively.

To demonstrate that the INAE proteins have DAG lipase activity, the INAE-A and -D protein isoforms were expressed in *E coli* and purified to >95% purity to carry out DAG lipase assays using 1-stearoyl-2-arachidonoyl-*sn*-glycerol as substrate, and the lipase assay products were analyzed by LC-MS (liquid chromatography-mass spectrometry) and GC-MS (gas chromatography-mass spectrometry) for identification of hydrolysis products and kinetic studies (Experimental Procedures).

LC-MS detected four products from the analysis of both INAE isoforms: two primary products, stearic acid (18:0) and 2-arachidonoyl glycerol (2-AG), and two minor products, arachidonic acid (20:4) and 1-stearoyl glycerol (1-SG), eluting at 6.3, 9.3, 5.8, and 8.7 min, respectively (Fig. 3B). Two primary products corresponded to hydrolysis at the *sn-1* position of DAG substrate and the two minor products corresponded to hydrolysis at the *sn-2* position (Fig. 3A). Thus, *in vitro*, the two recombinant INAE isoforms are both DAG lipases highly preferential for hydrolysis at the *sn-1* position, with the D form having much higher activity than the A form.

Enzyme kinetics were studied by GC-MS quantification of the lipase assay products. Amounts of liberated stearic acid and arachidonic acid were used to estimate the hydrolysis rates at the *sn-1* and *sn-2* positions, respectively (Fig. 3A). Enzyme kinetic characteristics were extracted from velocity dependence plots, plotting hydrolysis rates against substrate concentrations (Fig. 3C-a and b). In both INAE-D (Fig. 3C-a) and INAE-A (Fig. 3C-b), *sn-1* selectivity was about tenfold higher than that of *sn-2*. The kinetic values were calculated by pooling *sn-1* and *sn-2* data for each isoform (Fig. 3C-c). They were: V_{max} = 400.00 nmol/min-mg protein and K_m = 53.08 nmol (Y = 0.1327X + 0.0025, R_2 = 0.9906) for INAE-D, and V_{max} = 17.79 nmol/min-mg and K_m = 23.62 nmol (Y = 1.3278X + 0.0562, R_2 = 0.9377) for INAE-A (Fig. 3C-c). Thus, the D form represented about 20 fold higher lipase activity than the A form.

Molecular characterization of mutants and protein expression

The coding region and exon-intron boundaries of *inaE* were sequenced in both *N125* and *P19*. *N125* was found to harbor a G->A mutation at the 5′ splice site of the 13th intron (Fig. 2B). If splicing does not occur, translation would proceed into the 13th intron until a stop codon is encountered 39 bp downstream of the splice site. However, as described below, the mutation appears to be leaky. As for *P19*, no mutations were detected in either its *inaE* coding region or exon-intron boundaries. The P element insertion in *KG08585* is 20 bp downstream of the 5′ junction of the 13th intron (Flybase; Fig. 2C).

Polyclonal antibodies were raised against a 20-mer peptide near the C-terminal end of the INAE-A protein (Fig. 2C; Experimental Procedures) and are expected to recognize both isoforms of the INAE protein. In Western blots of wild-type heads, the antibody recognized two bands of approx. 70 and 110 kD (Fig. 4B). The heavier band migrated somewhat larger than the predicted molecular weight of ~90 kD. Neutralizing the antibody with excess amounts of the 20-mer peptide completely eliminated any recognizable bands in Western blots (results not shown), demonstrating the specificity of the antibody for the 20-mer peptide. Fig. 4B shows a representative set of Western blot data comparing the amounts of INAE proteins detected in *N125*, *P19*, and *KG08585* mutant heads with those in wild-type and *eya* (*eyes absent*) heads. Fig. 4C presents quantification of data based on three sets of measurements. The mutant *eya*, which has no eyes (Sved, 1986;Bonini, et al., 1997), had approximately 60 and 40% of the wild-type amounts of INAE-D and –A proteins, respectively, suggesting that INAE is expressed throughout the head, with substantial expression in the eye. All three *inaE* mutants, *N125*, *P19* and *KG08585*, had protein bands of the correct sizes but at reduced levels (~70–90% for INAE-D and 60–70% for INAE-A). The results suggested that all three mutants are relatively mild, partial loss-of-function mutants, $inaE^{N125}$ being the most severely affected of the three. The splice junction mutation in $inaE^{N125}$ appeared to be leaky, since apparently correctly spliced INAE proteins were produced at a reduced level.

The ERG phenotype reflected the mild nature of these mutations. *N125*, when placed on a white-eye background, consistently showed the slowly decaying ERG phenotype in response to a long white stimulus, shown in Fig. 1D. *P19* also generated decaying ERGs under similar conditions, but the amount of decay was about one half of that seen in *N125* and the phenotype was best seen after dark adaptation. However, *N125* and *P19* did not complement each other in complementation tests. None of the four P insertion mutants showed any obvious ERG phenotype, when tested as obtained on a w^+ background.

Subcellular distribution of the INAE protein

The polyclonal anti-INAE antibody was used in fluorescence confocal microscopy to examine the distribution of the INAE proteins in the eye. There was very little difference in the pattern of antibody labeling between *N125* and wild type except for the lower density of labeling in *N125*. Within the photoreceptors, the staining appeared as amorphous punctate material distributed unevenly throughout the photoreceptor cell body (Fig. 5A & B). Staining tended to be denser near the rhabdomeres (Fig. 5A), but it was not confined to any specific regions of the photoreceptor cell and seemed to be present throughout the length of the cell bodies (Fig. 5A & B). Although longitudinal images showed many labeled puncta that seemingly colocalized with rhabdomeres (Fig. 5B), most of these probably were located outside the rhabdomeres. Cross-sectional images also showed that most of the labeled puncta resided in photoreceptor cell bodies (Fig. 5A). Occasionally, however, some of the puncta were found localized within the rhabdomeres (arrowheads, Fig. 5A). Considering the geometry of rhabdomeres in cross-sectional images, the colocalizaiton was most likely real, suggesting that some of the INAE protein had access to the rhabdomeres.

Analysis of *inaE* mutants

Because the available *inaE* mutants were all hypomorphic, they were relatively uninformative in revealing the role of DAGL in phototransduction. We attempted to resolve this problem by (1) generating strong *inaE* mutant alleles, and (2) using a *norpA inaE* double mutant to limit the production of DAG and hence its metabolites during phototransduction.

A. Generation of strong *inaE* alleles—We generated strong *inaE* mutants by remobilizing the P element in the P insertion line, *KG08585* (Fig. 2B), to induce imprecise excision events. The offspring of 460 plus remobilization lines were examined by ERG (Experimental Procedures). None of the viable, excision-carrying progeny displayed severe ERG phenotypes. However, about 30 additional lines produced no viable offspring that were hemi- or homozygous for excision events. These results suggested that severe *inaE* mutations were homozygous lethal and that these mutations would have to be studied as somatic mosaics. Accordingly, we selected 25 of the lethal lines and generated, for each line, mosaic flies that were homozygous for imprecise excisions only in the eye using the *EGUF/hid* method of Stowers and Schwarz (1999) (Experimental Procedures).

Mosaic flies had slightly smaller than normal, mildly rough eyes (Stowers and Schwarz, 1999). Robust ERGs could be readily obtained from them, and the ERG phenotypes of the mosaic lines varied in severity. Three of these lines with ERG phenotypes varying from the mildest to severest, named *xl29, xl15,* and *xl18,* were chosen for analyses by electron microscopy, sequencing, real-time RT-PCR, and intracellular recordings.

A-1. Electron microscopy of *xls* (excision lines): The structural integrity of photoreceptors in *xl* mutants was examined by electron microscopy. Fig. 6 compares cross-sectional images of groups of *xl* and wild-type ommatidia taken at about 35 μm depth from the distal tips of rhabdomeres at 2–3 days post-eclosion. The size of *xl* eyes and cross-sectional areas of rhabdomeres were significantly smaller than those of wild type. Moreover, the *xl* ommatidia were less orderly in their arrangement than wild type, and many contained less than the normal complement of seven rhabdomeres. However, all these differences appeared to be common to all three *xl* mosaics. To quantify the variations in the number of rhabdomeres per ommatidium, the entire eye sections were viewed in low magnification EM to determine the fractions of ommatidia containing 7, 6, 5, etc. rhabdomeres. This was done on 3–4 different eyes for each genotype at the same depth of section and at the same age. The results are presented in Fig. 6B. There were no statistically significant differences in the percentage of ommatidia containing various numbers of rhabdomeres among the three *xl* mosaics. Thus, while distinct structural differences existed between *xl* mosaics and wild type, they were common to all three mosaics.

A-2. Molecular identification of alterations in *xl*: Because *xl* mutations are homozygous lethal in the adult, PCR amplifications for *inaE* gene sequencing or transcript quantification could not be performed in the adult. These were carried out in *xl* male embryos, which were viable and which could be identified through the use of a GFP-tagged balancer chromosome (Hagedorn et al., 2006; Experimental Procedures).

As in the case of *N125* (Fig. 1D), the rescue construct containing the D form of *inaE* cDNA rescued the mutant phenotype of *xl15* and *xl18.* The A form, while improving the phenotype slightly, was ineffective in rescuing it. By contrast, the lethality phenotype of *xl15* and *xl18* could be rescued by rescue constructs containing either the A or D form. However, the lethality of *xl29* could not be rescued by either form. The results suggested that the lethality-causing alterations generated by imprecise excision resided within the *inaE* coding sequences in *xl15* and *xl18*, but outside them in *xl29*. Consistent with this interpretation, no mutation was detected

in the *inaE* coding sequences of *xl29*. The most severely affected of the *xl* lines, *xl18*, carried a ~1.5 kb deletion extending from the middle of the 12th intron to near the beginning of the 14th intron, eliminating both the 13th and 14th exons (Fig. 7A). The deleted sequence was replaced by a ~690 bp translocation from the right arm of the third chromosome. *xl15* carried a >1.5 kb insertion that was too large to be amplified by PCR. The insertion site, determined within ~50 bp, was located just upstream of exon 13 (Fig. 7A).

A-3. RNA expression in *xl* mutants: The amounts of transcripts in *xl* mutants were determined by real-time RT-PCR of *xl* embryos (Experimental Procedures) and are shown normalized with respect to wild-type values of *inaE-D* transcript in Fig. 7B. The transcripts detected by primers common to both forms are shown normalized to the wild-type values within that series. *inaE-D* RNA expression in *xl29* was about 80% that of wild type and that of *xl15* was about 40%, while *xl18* had about 25% expression. *xl18* clearly is not a null mutant. Expression detected by primers common to both the A and D forms (5/6 in Fig. 7B) also showed a similar progressive decrease in relative amounts of RNA with severity of mutations.

B. Analysis of *norpA inaE* double mutants—The *norpA* gene encodes phospholipase C_β (Bloomquist et al., 1988), which catalyzes the hydrolysis of PIP_2 to DAG and IP_3 during phototransduction (Fig. 8A). In a *norpA inaE* double mutant, the *norpA* mutation limits the production of DAG, hence restricting the amount of DAG metabolites generated even if *inaE* is hypomorphic. In order to be able to monitor the effects of mutations by electrophysiology, we used a hypomorphic *norpA* allele, $norpA^{H43}$, which encoded a mutant PLC with ~7% of wild-type PLC activity that still allowed a receptor potential of sizable amplitude to be generated (Yoon et al., 2004). The amount of DAG generated in both the single and double mutants was expected to be very small compared to wild type because of the $norpA^{H43}$ mutation (Fig. 8A). If *inaE*, indeed, encoded DAGL that acted on DAG generated by *norpA*-encoded PLC, then, in the double mutant, the small amount of DAG generated would be inefficiently metabolized because of the $inaE^{N125}$ mutation. Thus, the amount of DAG metabolites generated was expected to be reduced and the amount of DAG was correspondingly increased in the double mutant compared to the single mutant. On the other hand, if *inaE*-encoded DAGL did not act on the DAG generated in the phototransduction cascade, introduction of *inaE* into the *norpA* background would have little or no effect on the NORPA-generated DAG.

The double mutants were generated using both the mild *N125* and the severe *xl18* alleles, and all recordings were performed intracellularly. As seen in Fig. 8B-i, a receptor potential of ~12.5 mV peak amplitude (~40% of wild-type amplitude) and ~6.5 mV steady-state amplitude could be elicited from $norpA^{H43}$ by a bright 10 s white stimulus. In the $norpA^{H43}$ $inaE^{N125}$ double mutant, on the other hand, the same stimulus elicited a receptor potential of comparable peak amplitude (11.5 mV) that rose to peak within 0.1 sec and rapidly and completely decayed to baseline within ~0.25 sec (Fig. 8B-i & ii). If *N125* is replaced with the severe *inaE* allele, *xl18*, in the double mutant, no response at all could be elicited (Fig. 8B-i & ii). Thus, under conditions in which the amount of DAG produced was restricted (hypomorphic *norpA* background), DAG metabolite(s) appeared to be required for the generation of the receptor potential.

C. Analysis of *xl* mutants—Shown in Fig. 8C are representative intracellular recordings of photoreceptor potentials elicited from the mosaic lines *xl29*, *xl15*, and *xl18*, by bright white stimuli of 30 sec duration. Quantification of various response parameters based on multiple recordings is presented in Table 2. The response parameters obtained from the *xl29* flies were indistinguishable from those of wild-type. Thus, the *xl29* data could be considered an internal wild-type control. By contrast, flies of the most severely affected of the three lines, *xl18*, gave only a small response of about 5 mV peak amplitude that rose slowly and decayed completely

to baseline in about 15 s (Fig. 8C-i & ii). It lacked both the maintained steady-state and the fast initial phasic components compared to *xl29* responses. Flies of the third mosaic line, *xl15*, responded with receptor potentials of intermediate phenotype. They had a small but distinct steady-state component of ~4 mV amplitude but lacked the rapidly rising, initial phasic component, present in *xl29*. Nevertheless, the initial rate of rise (activation rate) of the receptor potentials was substantially faster in *xl15* than *xl18* (Fig. 8C-ii; Table 2). These differences in receptor potential phenotype were observed reliably and consistently in multiple intracellular (n = 7–9, Table 2) and ERG recordings (n ≥ 15 each). Since no significant differences in morphological parameters were observed among these mutants, the phenotypic differences could not be attributed to structural differences.

We considered the possibility that blocking DAGL might have caused the DAG level to rise in *xl15* and *xl18* (Fig. 6A) leading to constitutive activity of TRP/TRPL channels (Raghu et al., 2000), collapse of the resting potential, and hence the degraded receptor potentials. Accordingly, resting potentials were determined for all three *xl* lines, $inaE^{N125}$ and $rdgA^{P35}$ single mutants, *norpA inaE* double mutants, as well as wild type. Resting potentials were difficult to determine in *rdgA* mutants, because strong depolarizations of cells made it difficult to judge penetration of cells reliably. The cells for which the resting potentials could be determined reliably tended to be less depolarized ones, biasing the sample toward larger resting potentials. Nevertheless, the average resting potential determined for $rdgA^{P35}$ was −43 mV, significantly smaller than the wild type value of −56 mV (Table 3). Likewise, resting potentials were smaller than normal in all lines heterozygous for Trp^{P365}, in which a substantial fraction of the TRP channels is expected to be constitutively active (Table 3). By contrast, resting potentials were normal in flies of all three mosaic lines (Table 3), ruling out collapse of the membrane potential as the basis of the small degraded responses of *xl15* and *xl18*.

Taken together, the above results suggested that the small degraded response obtained from *xl18* most likely had its origin in the residual DAGL activity in *xl18*, since it is not a null mutant. Furthermore, responses of the mosaic lines *xl15* and *xl29* were larger and faster because of the increasingly active presence of the DAGL, INAE.

D. Enhancement of Trp^{P365}/+ by $inaE^{N125}$—However, the above line of evidence seemingly contradicted the observation that the Trp^{P365}/+ phenotype was enhanced by $inaE^{N125}$ (Fig. 1C-b & 8D). As discussed earlier, placing $inaE^{N125}$ on a Trp^{P365}/+ background abolished the small receptor potential that remained in Trp^{P365}/+ (Fig. 1C-b; Fig. 8D). Since the reduction in size of the receptor potential in Trp^{P365}+ was due to constitutive activity of a substantial fraction of TRP channels (Yoon et al., 2000) and adding $inaE^{N125}$ was expected to increase the basal DAG level, a reasonable explanation was that DAG activated the remaining TRP channels. Consistent with this explanation, the resting potential was even more depolarized in $inaE^{N125}$; Trp^{P365}/+ than in Trp^{P365}/+ (Table 3). To understand this phenomenon further, we placed $inaE^{xl18}$, instead of $inaE^{N125}$, on a Trp^{P365}/+ background (Fig. 8D). Now a small receptor potential could be recovered from the double mutant (Fig. 8D; Table 2), and the resting potential also returned to the same level as in Trp^{P365}/+ (Table 3). Adding $inaE^{N125}$ to the Trp^{P365}/+ background would have increased DAG and decreased DAGL, and replacing it with $inaE^{xl18}$ would have sharply enhanced these conditions. Thus, the above results were opposite of what one would expect if DAG were excitatory to the channels.

Discussion

A growing body of evidence suggests that *Drosophila* phototransduction utilizes the DAG branch of the G-protein-coupled, PLC_{β}-mediated signaling pathway (reviews: e.g., Hardie, 2003). Although DAG lipase is expected to play a critical role in this pathway, no DAG lipase that could play such a role had been identified previously in *Drosophila*. Here we report on a

DAG lipase identified from the *Drosophila* mutants, *inaE*. The *inaE* gene was found to encode two protein isoforms, INAE-A and INAE-D, by alternative splicing. Both these proteins are highly homologous to the two previously identified mammalian *sn-1* type DAG lipases, and *in vitro* DAG lipase assays of recombinant INAE-A and INAE-D showed that both are DAG lipases highly preferential for hydrolysis at the *sn-1* position (Fig. 3). Expression of the INAE protein is not restricted to the eye but occurs throughout the head (Fig. 4A & B), consistent with the finding that strong mutations in this gene are homozygous lethal. In photoreceptors, anti-INAE antibody labeling occurs as punctate staining scattered throughout the photoreceptor cytoplasm (Fig. 5A). Occasionally, some of the puncta are found within the rhabdomeres, indicating that some DAGL enters the rhabdomeres. Results of the *norpA inaE* double mutant study (Fig. 8B) provide strong functional support for the above observation. In this study, the receptor potential disappears in an *inaE* allele-dependent manner – the stronger the *inaE* allele in the double mutant, the more severe the double mutant phenotype. The allele dependence strongly suggests that the action of *inaE*-encoded DAGL is responsible for the observed double mutant phenotype. Furthermore, to affect the receptor potential phenotype, DAGL must act on the DAG generated by *norpA*-encoded PLC_{β}, and, for that to occur, DAGL must enter the rhabdomeres.

Because *inaE* mutations already available were all relatively mild, severe mutations were generated by imprecise excisions of a P element insertion in the *inaE* gene. These imprecise excision alleles were homozygous lethal and had to be studied as eye mosaics. Quantitative RT-PCR results showed that even the severest of these imprecise excision mutants, $inaE^{xl18}$, is not a null mutant and expresses RNA at ~25% of the normal level. This mutation profoundly affects the photoreceptor responses to light. If *xl18* is placed on a $norpA^{H43}$ background to reduce the amount of DAG generated, the light stimulus generates no response at all (Figs. 8B). In *xl18* flies themselves, a bright prolonged stimulus generates only a small response of slow kinetics that decays to baseline completely during the stimulus (Fig. 8C). This response most likely represents the residual DAGL activity in this severely affected mutant. As the severity of mutation progressively decreases in the *xl* series of mutants, the receptor potential phenotype returns to normal in an allele-dependent manner (Fig. 8C). Again, the *inaE* allele-dependence strongly argues that the action of *inaE*-encoded DAGL is responsible for the observed change in the receptor potential phenotype. These results, taken together, thus, suggest (1) that the production of DAG metabolite(s) through the action of the *inaE*-encoded DAGL is required for the generation of photoreceptor responses to light and (2) that, in the absence of the metabolite, DAG plays little direct role in the activation of channels. However, the identity of the excitatory molecule cannot be specified from this work. It could be one or more of the products generated by INAE, such as monoacylglycerol (2-AG) or stearic acid (Fig. 3A), or even DAGL (INAE) itself.

While DAG may not have a direct role in channel activation, we found evidence suggesting that it may be important in regulating the action of the DAG metabolite that acts as an excitatory agent, although the evidence is still largely indirect. As discussed earlier, the ability of $inaE^{N125}$ to act as an enhancer of Trp^{P365}/+ (Fig. 1D-b; 8D) seems to present a quandary when considered in relation to the results summarized above. If DAG has little or no direct role in channel activation, how does one explain the disappearance of the small response present in *P365*/+ when *N125* is added to this background (Figs. 1C-a & b; Fig. 8D, bottom trace)? A simple explanation for the phenomenon would be that DAG is excitatory to the channels and that adding *N125* to the *P365*/+ background raised the level of DAG to make more channels to become constitutively active in *N125;P365*/+ than in *P365*/+. However, results of the experiment replacing *N125* with a stronger *inaE* allele, *xl18*, in the *N125;P365*/+ double mutant (Fig. 8D) run counter to this simple explanation. Replacing *N125* with *xl18* should have sharply raised the basal DAG level further in the double mutant. If DAG were excitatory, the resting potential should have depolarized even more than before the *N125* replacement and no receptor

potential at all should have been obtained. Just the opposite results were obtained. A small but distinct receptor potential could be recorded from *xl18;P365*/+ (Fig. 8D, middle trace), and the resting potential has returned to the level in *P365*/+ (Table 3). These results are incompatible with the hypothesis that DAG is excitatory to the channel and instead provides another line of evidence for the conclusions summarized earlier.

However, the fact that a much more severe phenotype is obtained in *N125;P365*/+ than in *P365*/+ or *xl18;P365*/+ suggests that DAG may have a role in facilitating, enhancing and orchestrating the action of the DAG metabolite that serves as the excitatory agent. This action of DAG would be more noticeable under conditions in which a sufficient amount of the excitatory product is produced, as in *N125;P365*/+ than in *xl18;P365*/+. A similar action of DAG can also be inferred from the *norpA inaE* double mutant studies (Fig. 8B). In this series of experiments, hypomorphic *norpA* mutation, *H43*, was used to restrict the amount of DAG generated both in the single and double mutants. The response obtained from *H43 N125* is short in duration but has nearly the same maximum amplitude as the *H43* response and much faster time course of rise than the *H43* response (Fig. 8B). The shortness of response duration may be due to the fact that under the conditions of this experiment (restricted DAG generation), the response cannot be sustained during a bright prolonged stimulus. This response arises as a result of DAGL activity because further reducing the DAGL activity (*xl18* mutation) abolishes the response (Fig. 8B). However, the fact that adding *N125* to the *H43* background resulted in a response of faster time course may also be a manifestation of the enhancing and facilitatory effects of DAG on the excitatory agent. Speculating further, the facilitatory action of DAG might be in place to ensure that the excitation of channels is light-regulated since DAGL activity is not light-regulated while the generation of DAG is.

Experimental Procedures

Experimental animals

The wild-type strains were Berlin and Oregon R marked with *white (w)*. Both $inaE^{P19}$ and $inaE^{N125}$ were recovered in ethylmethane sulfonate mutagenesis in the 70's, *P19* in the Pak laboratory and *N125* by Martin Heisenberg, in Tübingen, Germany. The P-insertion mutant *KG08585* was obtained from the Bloomington Stock Center. The *xl* mutants were obtained by inducing imprecise excision through remobilization of the P element insertion in the *KG08585* mutant.

Microarray analysis, statistical analysis and candidate gene identification

Three independent replicate RNA samples (>5 μg) each were prepared from $inaE^{N125}$ and a wild-type control. Total RNA was extracted from isolated heads using the RNeasy mini kit (Qiagen), and each sample was checked for quality and concentration before being handed over to the Center for Medical Genomics, Indiana University School of Medicine for processing. The chips used were the Affymetrix "GeneChip *Drosophila* Genome 2.0 Arrays," based on *Drosophila* Genome Annotation release 3.1 and each comprising 18,952 probe sets. The processing of samples was all carried out by the Center according to the Affymetrix protocol (http://www.affymetrix.com/Auth/support/downloads/manuals/expression_s2_manual.pdf).

Statistical analysis of data, carried out by LA and RWD, consisted of using an analysis of variance (ANOVA) to statistically test for differences in mRNA steady-state levels between the mutant and the control using normalized data (Craig et al., 2003). It was necessary to adjust for the type I error rate to accommodate multiple testing issues, using both the false discovery rate (FDR) approach (Benjamin and Hochberg, 1995) and Holm's sequential Bonferroni correction procedure (Holm, 1979). The significance level was chosen as 0.05.

Candidate genes for *inaE* were identified by looking for those genes within the mapped region that showed the largest and/or most statistically significant changes in the mRNA level in $inaE^{N125}$compared to wild type. The Affymetrix Drosophila 2.0 annotation file was used to determine the identity of genes corresponding to probe sets detecting significant alterations in the mRNA level (http://www.affymetrix.com/support/technical/byproduct.affx?product=fly-20).

Validation of gene identification: rescue constructs

Total RNA was extracted from Berlin (wild type) fly heads, and cDNA was synthesized using the Superscript II reverse transcriptase and a primer mix of oligo $(dT)_{15}$ and $d(N)_6$ (Invitrogen).The cDNA for *inaE-RA* and *inaE-RD* were amplified from Berlin head cDNA using high fidelity pfuTurbo DNA polymerase (Stratagene). The *inaE-RA* and *inaE-RD* clones were completely sequenced for accuracy and extracted by endo-free plasmid maxi kit (Qiagen). They were cloned into the *pCaSpeR*[*trp*, *w+*] vector at the *Xba*I and *Bgl*II sites, allowing expression of the inserts to be driven by the *trp* promoter. The constructs were injected into $inaE^{N125}$ mutant embryos.

Electrophysiology

Light stimuli originated from a 300 W Halogen lamp (OSRAM) and were delivered to the specimen with a light guide, using neutral density filters to achieve desired intensity, when needed. The unattenuated intensity at the level of the fruitfly was 810 $\mu W/cm^2$. Both the recording and ground electrodes were filled with Hoyle's solution. Orange and blue stimuli were generated by interposing, respectively, Corning CS2-73 and 5433 filters in the light path without attenuation. For other purposes, unattenuated white stimuli were used. All ERG recordings were performed at 25°C.

Intracellular recordings were performed as described in Johnson and Pak (1986). Both the ground and recording electrodes were inserted through a small cut made in the corneal-head junction. The recording electrode had 25–50MΩ resistance when filled with 2M KCl. The light source and the filters were as in ERG recordings. Signals were sampled at 2 kHz with an analog-to-digital converter (Digidata 1200A), and the data were acquired and analyzed with Axoscope software (Axon Instruments).

Expression of recombinant INAE-PD and INAE-PA

The *inaE-RA* and *inaE-RD* sequences were ligated onto the *pET24a* expression vector (Novagen) containing a C-terminal 6×His tag. Recombinant INAE-PA and INAE-PD were expressed in *E. coli* Rosetta (DE3) (Novagen) according to the standard protocol. The recombinant INAE protein isoforms were purified in a Ni-NTA agarose column (Qiagen) from the soluble fraction of the *E. coli* cell culture according to the manufacturer's instructions. The recombinant proteins were concentrated by Amicon Ultrapure-15 centrifugal filter (Sigma) with exchange of buffer to 20 mM MOPS, pH 7.0. Corresponding fractions from the products of *E. coli* containing empty vectors served as negative controls. SDS-PAGE analysis indicated that the purity of the recombinant proteins obtained was >95%.

Diacylglycerol Lipase Assay

Using 1-stearoyl-2-arachidonoyl-*sn*-glycerol (Sigma) as substrate, assays were performed at 37 °C for 15 min in 20 mM MOPS buffer (pH 7.0) containing 0.25% (w/v) fatty acid-free bovine serum albumin (BSA) (Sigma) and 0.5% (w/v) gum arabic (Sigma). 20 μg recombinant proteins (INAE-PD or INAE-PA) were used per assay in 0.5 ml of reaction mixture. The substrate (10% w/v) was emulsified in 10 % (w/v) gum arabic and diluted into the reaction

mixture to the final amounts of substrate. Assay products were extracted by chloroform/methanol (1:2, v/v) for molecular species analysis by LC-MS and kinetic analysis by GC-MS.

High performance liquid chromatography–mass spectrometry (LC-MS)

The HPLC-MS system consisted of an Agilent series 1100 HPLC coupled to an Agilent 6210 LC-TOF mass spectrometer via ESI interface. Reversed phase HPLC separation was conducted on a Zorbax SB-C8 column (50 mm × 4.6 mm I.D., 3.5 μm) (Agilent) at a flow rate of 1.0 ml/min using a gradient mobile phase. The mobile phase initially consisted of acetonitrile, water, and ammonium acetate in the following proportions: 45:55:0.1 (v/v/w). The acetonitrile fraction was then increased to 90% in a linear gradient over 10 min, and then held at 90 % for 10 min. The column was maintained at 35 °C. The MS system was operated in the negative ion mode with capillary temperature of 350 °C and capillary voltage of 4 kV. The spectra were recorded in the *m/z* 50–1699 range.

Gas liquid chromatography–mass spectrometry (GC-MS)

Samples were TBDMS-derivatized by adding anhydrous pyridine (Sigma) and MTBSTFA (Regis Technologies) and heating at 60 °C for 1 hr. GC-MS was performed using an Agilent 6890N model gas chromatograph interfaced to a LECO Pegasus III TOF-MS (LECO Corp.). A 30 m × 0.25 mm I.D., 0.25 μm HP-5MS capillary column (Agilent) was used under the following conditions: injector temperature, 280 °C; GC column temperature, 225 °C for 2 min, then 8 °C/min to a final temperature of 300 °C and held for 15 min; transfer-line temperature, 280 °C; ion-source temperature, 200 °C; and carrier gas, helium. Analyses were performed in the electron ionization (EI) mode at 70 eV. Mass spectra were acquired in the *m/z* 50–900 range.

Polyclonal antibody

Polyclonal anti-*inaE* antibodies were raised in rabbit against the 20-mer peptide (TARSTSAHPTDSSIALTLHQ), located within the peptide encoded by exon 12 (Fig. 2C). The antibody was purified by affinity chromatography using INAE peptide-conjugated agarose beads (Bethyl).

Confocal microscopy

Heads of 1 d-old flies were immersed in the fixative (2% paraformaldehyde, 0.21% sodium m-periodate, 1.37% DL-lysine, 0.001g saponin in 1 ml PBS buffer) overnight at 4°C. Eyes were dissected out and allowed to continue fixation for 1 hr at 4°C in the same fixative. Dissected eyes were washed 3x in PBST (phosphate buffered saline, 0.05% Tween20) and blocked for 2 hour in PBST/4% BSA/10% normal donkey serum. They were incubated in an anti-INAE antiserum diluted 1: 150 with PBS containing 4% BSA and 10% normal donkey serum overnight at 4°C. For actin staining, Texas Red-conjugated phalloidin (Molecular Probes) was added to the diluted primary antiserum in a ratio of 1:100. After 3x PBST washes, eyes were incubated for 4 hours at room temperature in donkey anti-rabbit IgG labeled with Alexa Fluor 488 (Molecular Probes) diluted 1:200 with PBS containing 4% BSA and 10% normal donkey serum. Specimens were washed 3x in PBST, mounted with ProLong Gold Antifade Reagents (Molecular Probes), and viewed on a Bio-Rad MRC1024 confocal microscope (Nikon 60x, 1.4NA lens).

Electron microscopy

Heads of adult flies were bisected and immersed in the primary fixative (2.5% glutaraldehydde and 2% paraformaldehyde in 0.1 M cacodylate buffer, pH 7.4) and post-fixed in reduced OsO4 (1% OsO4 + 1.5% $K_3Fe(CN)_6$). The tissue was dehydrated in a graded ethanol/water series (10, 30, 50, 70, 90, and 2× 100% ethanol, 40 s each), followed by an exchange of ethanol with

propylene oxide, infiltrated with Epon/Spurr (1:1) in graded mixtures with propylene oxide (25, 50, 75%, 2 hr each, 100% Epon/Spurr, 6 hr), imbedded in Epon/Spurr in a pyramid-tip mold, and polymerized for 48 hr at 60°C. Fixation and infiltration were accelerated by microwaving. Blocks were sectioned on Leica EM UC6 with a low-compression Diatome diamond knife, sections were stained with uranyl acetate followed by lead citrate, and images were viewed on the FEI/Philips CM-10 Biotwin transmission electron microscope (FEI/Philips, Hillsboro, OR).

Generation of imprecise excision lines (*xl*)

The P element in the P insertion line *KG08585* (Fig. 2B) was mobilized by crossing the *KG08585* stock with the (*Δ2–3*) stock. To track each excision event independently, balanced virgin female offspring carrying a P element excision were mated individually to males of the balancer stock to establish ~500 single female P-excision lines. All lines that produced viable male progeny hemizygous for excision were tested by screening for ERG phenotypes, and they all gave normal or nearly normal ERGs. However, there were about 30 lines that produced no viable males that are hemizygous for P excision events. Twenty-five of these homozygous lethal excision lines (*xl* lines) were used to make mosaic flies that are homozygous for *xl* only in the eye using the *EGUP/hid* method.

Generation of mosaic flies

Generation of mosaic flies followed the *EGUF/hid* method of Stowers and Schwarz (1999). In this method, a combination of the *FRT/FLP* and *GAL4/UAS* systems is used to induce, only in the eye, mitotic recombination between the chromosome carrying a lethal mutation of interest (*xl* in this case) and the *GMR-hid*-carrying chromosome. Mitotic eye clones that are not homozygous for *xl* are killed off by the dominant photoreceptor lethal transgene *GRM-hid*, resulting in adult eyes homozygous only for *xl*. Site specific recombination is achieved by recombining the flipase recognition site *FRT* in each of the *xl*- and *GMR-hid*-carrying chromosomes and providing the site specific recombinase *FLP* activity in precursor eye cells (driven by the eyeless promoter) through the use of the *EGUF* (*eyeless Gal4 UAS FLP*) stock available from the Stock Center. The mosaic flies had the genotype, *xl FRT/GMR-hid FRT;;EGUF/EGUF*. The *GMR-hid FRT;;EGUF/EGUF* stock obtained from the Bloomington Stock Center was used to recombine *FRT* into the *xl*-carrying chromosome and to construct the mosaic flies.

Sequencing *xl* embryos

Since *xl*s are homozygous lethal in the adult and *xl* stocks are kept over the *FM7a* balancer, one cannot sequence the *inaE* gene in the adult. Sequencing was carried out in *xl* embryos, which were viable, using a modification of the procedure described by Hagedorn et al. (2006). The *FM7a* balancer which was normally used to balance the *xl* stocks (*xl/FM7a* × *FM7a*/⁀) was replaced with the *FM7c-Kr*-GFP balancer, which had the GFP-tagged *Krüppl* gene inserted into the balancer chromosome. Thus, the stock was kept as (*xl/FM7c Kr*-GFP × *FM7c Kr*-GFP/⁀). *Krüppl*-GFP is expressed in >3 hr old embryos, and all embryos carrying the balancer fluoresce at >3 hr. The only embryos that do not fluoresce are males hemizygous for *xl*. These were identified under a fluorescence microscope (Olympus SZX7) at 10 hr and used in sequencing.

Quantitative RT PCR of *xl* mutants

For the same reason given above, Quantitative RT PCR also had to be carried out on embryos. Total RNA was extracted from ~5 embryos using Qiagen RNeasy mini kit, and Verso^{TM} SYBR Green 1-Step QRT-PCR ROX kit was used for the preparation of the reaction mixture. Measurements were carried out on the Applied Biosystems 7300 real-time PCR unit, and the

ABI7300 system software was used for data analysis. The following primer pairs were used. Primers 1 and 2 (*inaE-D* specific): (5′TCGTGTCTTGTAGAGATCGA3′) and (5′ TTATATAGAAGGCGGGCGGC3′); primer pairs 3/4 (*inaE-A* specific): (5′ TCATCCCAAGCCCGACGAGCA3′) and (5′ATGCGCTTTGTAGGTGTGTG3′); primer pairs 5/6 (both *inaE-A*& *-D*): (5′TTGTTAGCGTCTCGTTGGTT3′) and (5′ AGGTGCACCATATCGTGATT3′); RP49: (5′CGGTTACGGATCGAACAAGCG3′) and (5′ TTGGCGCGCTCGACAATCT).

Supplementary Material

Refer to Web version on PubMed Central for supplementary material.

Acknowledgements

We thank Kim Gilbert for help with the manuscript preparation, Chaoxian Geng and Guohua Li for their contributions in the early phases of the work, and Eric Harness, Junko Kitamoto, and Chia-Ping Huang for their technical assistance. The $inaE^{N125}$ mutant was a generous gift from Martin Heisenberg in the 70's. We gratefully acknowledge the receipt of $Df(1)ben^{C02}$, *Df(1)AR10, FM7c Kr-GFP, and Yp3* stocks from Howard Nash, John Thomas, Henry Chang, and Mary Bownes, respectively. Other stocks were obtained from the Bloomington Stock Center. The microarray work was carried out in the Center for Medical Genomics, Indiana University School of Medicine (Director: Howard Edenberg). Confocal microscopy was carried out in the departmental confocal facility (Director: Don Ready), the sorting of *xl* mutant embryos were carried out in Henry Chang's laboratory, electron microscopy was carried out in Purdue University Life Science Microscope Facility (Director: Debra Sherman), and lipase assays were performed in Purdue Metabolomics Profiling Facility. We gratefully acknowledge the help of Don Ready, Henry Chang, and Bruce Cooper. This work was supported by NEI grant EY00033 to WLP.

References

Acharya JK, Jalink K, Hardy RW, Hartenstein V, Zuker CS. $InsP_3$ receptor is essential for growth and differentiation but not for vision in Drosophila. Neuron 1997;18(6):881–887. [PubMed: 9208856]

Benjamini Y, Hochberg Y. Controlling the false discovery rate: A practical and powerful approach to multiple testing. J Royal Stat Soc B 1995;57:289–300.

Bisogno T, Howell F, Williams G, Minassi A, Cascio MG, Ligresti A, Matias I, Schiano-Moriello A, Paul P, Williams E-J, Gangadharan U, Hobbs C, Di Marzo V, Doherty P. Cloning of the first sn1-DAG lipases points to the spatial and temporal regulation of endocannabinoid signaling in the brain. J Cell Biol 2003;163(3):463–468. [PubMed: 14610053]

Bloomquist BT, Shortridge RD, Schneuwly S, Perdew M, Montell C, Steller H, Rubin G, Pak WL. Isolation of a putative phospholipase C gene of Drosophila, norpA, and its role in phototransduction. Cell 1988;54:723–733. [PubMed: 2457447]

Bonini NM, Bui QT, Gray-Board GL, Warrick JM. The Drosophila eyes absent gene directs ectopic eye formation in a pathway conserved between flies and vertebrates. Development 1997;124(23):4819–4826. [PubMed: 9428418]

Chyb S, Raghu P, Hardie RC. Polyunsaturated fatty acids activate the Drosophila light-sensitive channels TRP and TRPL. Nature 1999;397:255–259. [PubMed: 9930700]

Craig BA, Black MA, Doerge RW. Gene expression data: The technology and statistical analysis. J Agric Biol and Environ Stat 2003;8(1):1–28.

Hagedorn EJ, Bayrakta JL, Kandachar VR, Bai T, Englert DM, Chang HC. Drosophila melanogaster auxilin regulates the internalization of Delta to control activity of the Notch signaling pathway. J Cell Biol 2006;173(3):443–452. [PubMed: 16682530]

Hardie RC. Regulation of TRP Channels via Lipid Second Messengers. Annu Rev Physiol 2003;65:735–759. [PubMed: 12560473]

Hardie RC. TRP channels and lipids: from Drosophila to mammalian physiology. J Physiol 2007;578:9–24. [PubMed: 16990401]

Hardie RC, Martin F, Cochrane GW, Juusola M, Georgiev P, Raghu P. Molecular basis of amplification in Drosophila phototransduction: roles for G protein, phospholipase C, and diacylglycerol kinase. Neuron 2002;36:689–701. [PubMed: 12441057]

Holm S. A simple sequentially rejective multiple test procedure. Scand J Stat 1979;6:65–70.

Huang FD, Matthies HJ, Speese SD, Smith MA, Broadie K. Rolling blackout, a newly identified PIP_2-DAG pathway lipase required for Drosophila phototransduction. Nat Neurosci 2004;7:1070–1078. [PubMed: 15361878]

Johnson EC, Pak WL. Electrophysiological study of Drosophila rhodopsin mutants. J Gen Physiol 1986;88:651–673. [PubMed: 3097245]

Leung, H-T.; An, L.; Tseng-Crank, J.; Kim, E.; Harness, EL.; Zhou, Y.; Kitamoto, J.; Li, G.; Doerge, RW.; Pak, WL. Phototransduction in Drosophila: Use of microarrays in cloning genes identified by chemically induced mutations causing ERG defects. In: Fliesler, SJ.; Kisselev, OG., editors. Signal Transduction in the Retina. Boca Raton, FL: CRC Press; 2007. p. 195-217.

Masai I, Okazaki A, Hosoya T, Hotta Y. Drosophila retinal degeneration A gene encodes an eye-specific diacylglycerol kinase with cysteine-rich zinc-finger motifs and ankyrin repeats. Proc Natl Acad Sci USA 1993;90:11157–11161. [PubMed: 8248222]

Minke, B. Cell Calcium. 40. 2006. TRP channels and Ca^{2+} signaling; p. 261-275.Review

Montell C. The TRP Superfamily of Cation Channels. Sci STKE 2005;2005:re3. [PubMed: 15728426]

Raghu P, Colley NJ, Webel R, James T, Hasan G, Danin M, Selinger Z, Hardie RC. Normal phototransduction in Drosophila photoreceptors lacking an $InsP_3$ receptor gene. Mol Cell Neurosci 2000;15:429–445. [PubMed: 10833300]

Raghu P, Usher K, Jonas S, Chyb S, Polyanovsky A, Hardie RC. Constitutive activity of the light-sensitive channels TRP and TRPL in the Drosophila diacylglycerol kinase mutant, rdgA. Neuron 2000;26:169–179. [PubMed: 10798401]

Stowers RS, Schwarz TL. A genetic method for generating Drosophila eyes composed exclusively of mitotic clones of a single genotype. Genetics 1999;152:1631–1639. [PubMed: 10430588]

Sved J. Eyes absent (eya). Drosophila Inform Serv 1986;63:169.

Yoon J, Ben-Ami HC, Hong YS, Park S, Strong LLR, Bowman J, Geng C, Baek K, Minke B, Pak WL. Novel mechanism of massive photoreceptor degeneration caused by mutations in the trp gene of Drosophila. J Neurosci 2000;20(2):649–659. [PubMed: 10632594]

Yoon J, Leung H-T, Lee S, Geng C, Kim Y, Baek K, Pak WL. Specific molecular alterations in the norpA-encoded phospholipase C of Drosophila and their effects on electrophysiological responses in vivo. J Neurochem 2004;89:998–1008. [PubMed: 15140198]

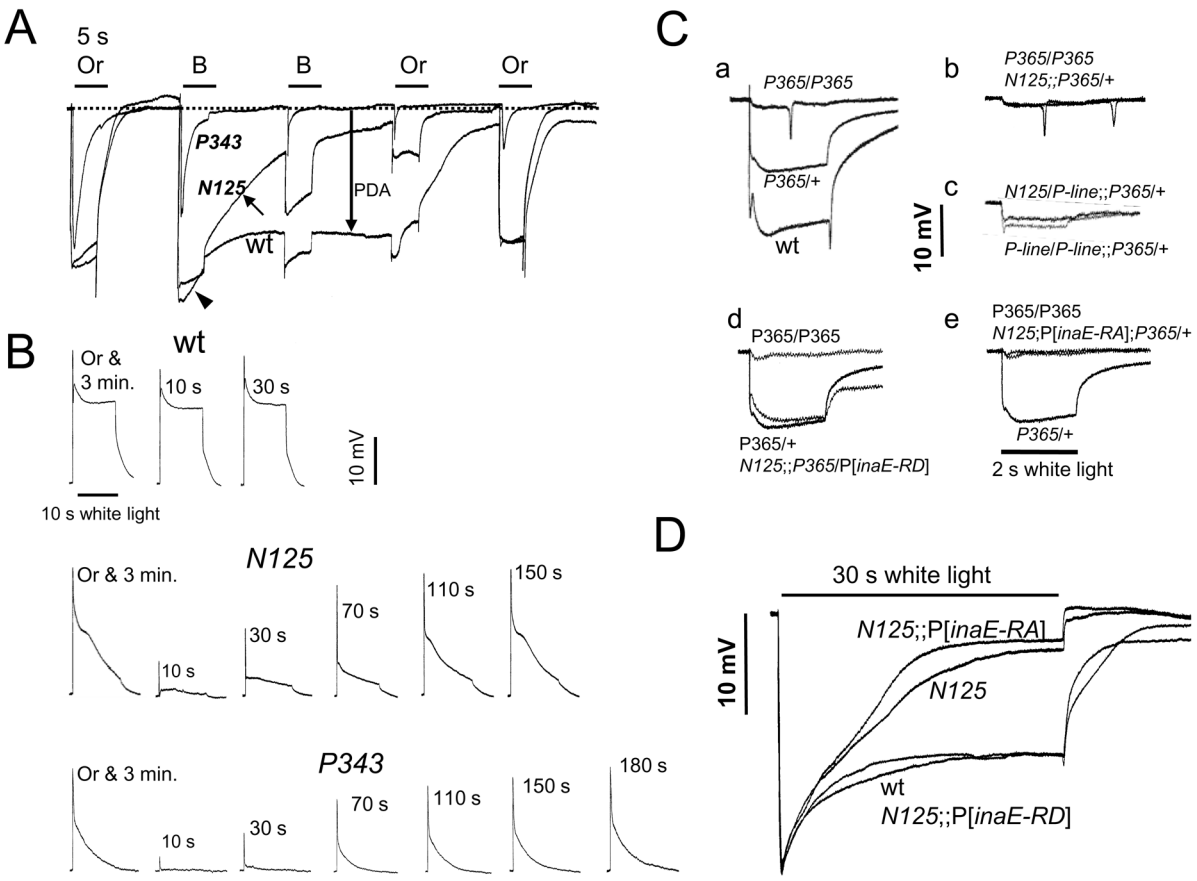

Fig. 1. ERG analyses of *inaE*^{N125}

A) Comparison of ERG phenotypes of *inaE*^{N125} (*N125*), *trp*^{P343} (*P343*), and wild type (wt). ERGs recorded from wild type, *inaE*^{N125}, and *trp*^{P343} are shown superimposed. The *inaE*^{N125} phenotype fell between those of wild type and *trp* in severity. B, Or: blue and orange stimuli generated by interposing, respectively, Corning 5433 and CS2–73 filters in the light path. **B)** Comparison of refractory periods among wild type, *inaE*^{N125}, and *trp*^{P343}. For each genotype, the fly was given a 5 s orange stimulus and allowed to dark adapt for 3 min before being exposed to the first stimulus. Immediately after the first stimulus, a 5 s orange stimulus was given and the second stimulus was delivered after a dark duration of 10, 30, 70, 110, 150, or 180 s. **C-a)** Semidominance of *Trp*^{P365} (*P365*). *P365* heterozygotes (*P365/+*) generated responses that were about half-way between those of wild type and *P365* homozygotes in size. **C-b)** Enhancement of *P365/+* by *N125*. **C-c)** Non-complementation between *KG08585* (P-line) and *N125*. *KG08585* enhanced the *P365/+* phenotype. Moreover, a heteroallelic combination of *KG08585* and *N125* also enhanced *P365/+*. **C-d,e)** The interaction between *inaE*^{N125} and *Trp*^{P365} was nullified by the expression of the D form **(d)** but not the A form of INAE. **(e). D)** Rescue of the *inaE*^{N125} ERG phenotype by the rescue construct harboring the *inaE-RD* isoform but not by that containing the *inaE-RA* isoform. Quantification of the above data based on multiple recordings is presented in Table 1.

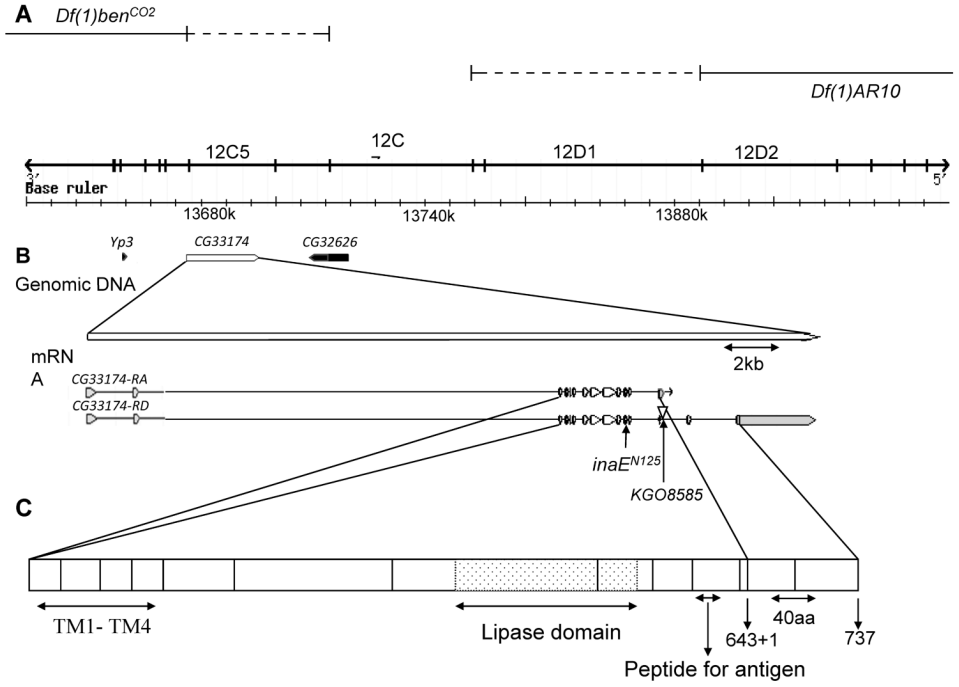

Fig. 2. Maps of the *inaE* region, gene, transcript, and protein

A) The *inaE* genomic region. *inaE* mutations are uncovered by the deficiencies *Df(1)ben*^{CO2} (first line) and *Df(1)AR10*(second line). The third line shows cytogenetic regions, and the fourth line indicates nucleotide coordinates. **B)** The *CG33174* (*inaE*) gene and its transcripts. *Yp3* and *CG32626*, shown in black, were identified along with *CG33174* in microarrays as potential candidate genes. The *inaE* gene generates two transcripts, *RA* and *RD*, by alternative splicing. In the A form, the 13th intron is not spliced out and transcription ends in the 13th intron, thereby adding one amino acid residue to the A form of the protein (indicated by "643 + 1" in **(C)).** Untranslated regions are shown in grey. The sites of the *inaE*^{N125} mutation and of *KG08585* insertion are indicated. **C)** The INAE protein. The regions of the four transmembrane segments and the lipase domain, as well as the 20-mer peptide used in antibody generation, are indicated. The C-termini of the A and D forms of the INAE protein are indicated by arrows and the C-terminal amino acid residue number. The vertical lines correspond to coding exon boundaries.

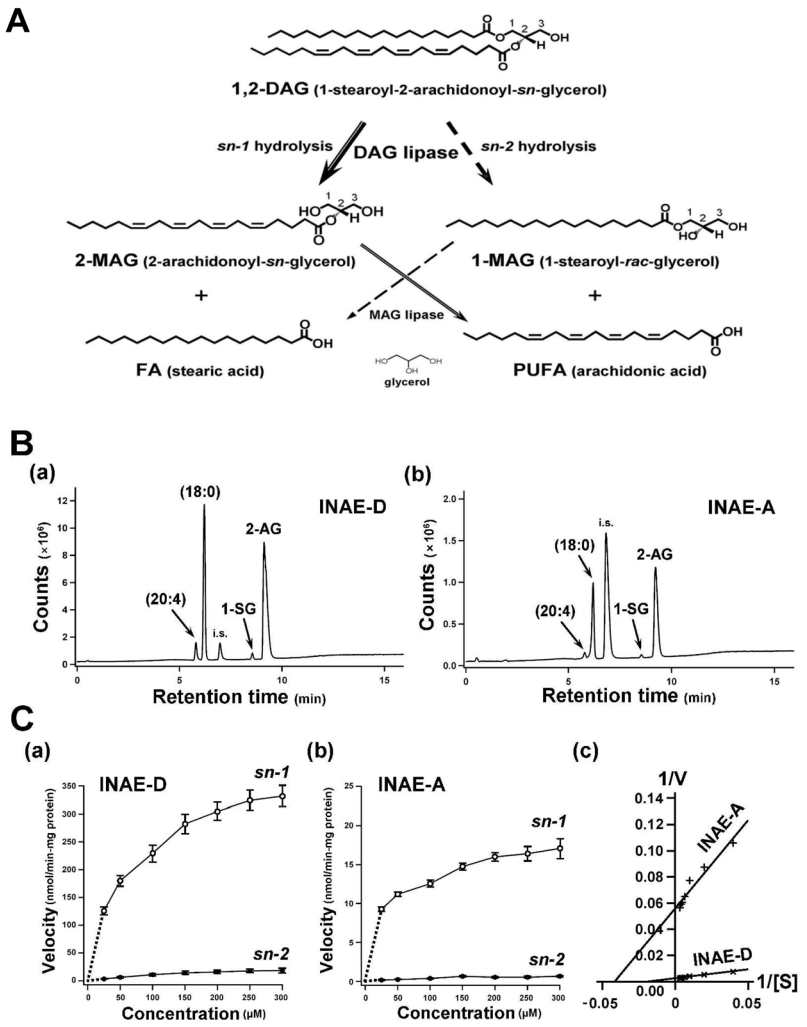

Fig. 3. DAG lipase assay

A) Potential metabolic pathways of the DAG substrate. **B)** Enzymatic characterization of INAE isoforms. Representative LC-MS total ion chromatograms (*m/z* 65–500) of INAE-D **(B-a)** and INAE-A **(B-b)** lipase assay products, using 1-stearoyl-2-arachidonoyl-*sn*-glycerol as substrate. Arachidonic acid (20:4), stearic acid (18:0), 1-stearoyl glycerol (1-SG), and 2-arachidonoyl glycerol (2-AG) were eluted at 5.8, 6.3, 8.7, and 9.3 min, respectively. Samples contained palmitic acid as an internal standard (i.s.). **C)** Velocity dependence plots as a function of substrate concentration obtained by GC-MS. Assays were performed on recombinant INAE-D **(C-a)** and INAE-A **(C-b)** using the same substrate as in **(B)**. Hydrolysis rates at *sn-1* and *sn-2* positions were estimated by the amount of released stearic acid and arachidonic acid, respectively (Fig. 3A). Open and closed circles represent *sn-1* and *sn-2* reactions, respectively. Values represent the mean ± SD (n = 4). Note that the ordinate scales are different between **(B-a)** and **(B-b)** and between **(C-a)** and **(C-b). C-c)** Determination of kinetic parameters by Lineweaver-Burk plots. Calculations were performed by pooling *sn-1* and *sn-2* data for each isoform. V: velocity; [S]: substrate concentration.

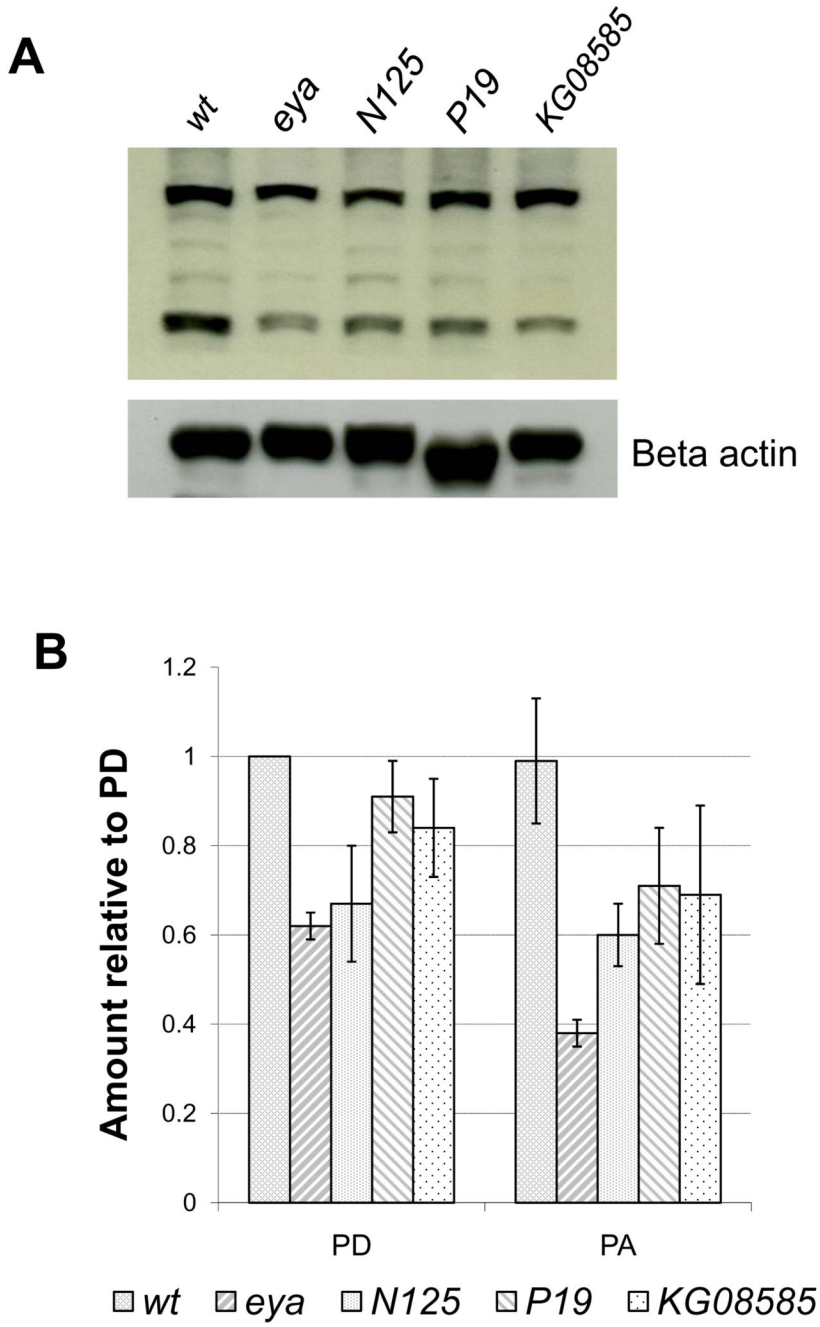

Fig. 4. Western blot analysis of *inaE* mutants with *eya* and wt controls

A) A representative blot obtained in Western blot analyses carried out on the isolated heads of the *inaE* mutants, *N125, P19,* and *KG08585*. Beta actin was used as loading control; *eya: eyes absent*. **B)** Quantification of the data. Each data point was normalized with respect to the corresponding beta actin loading control, and the normalized data points in a given blot were in turn normalized to the wild-type PD value. Based on three repetitions.

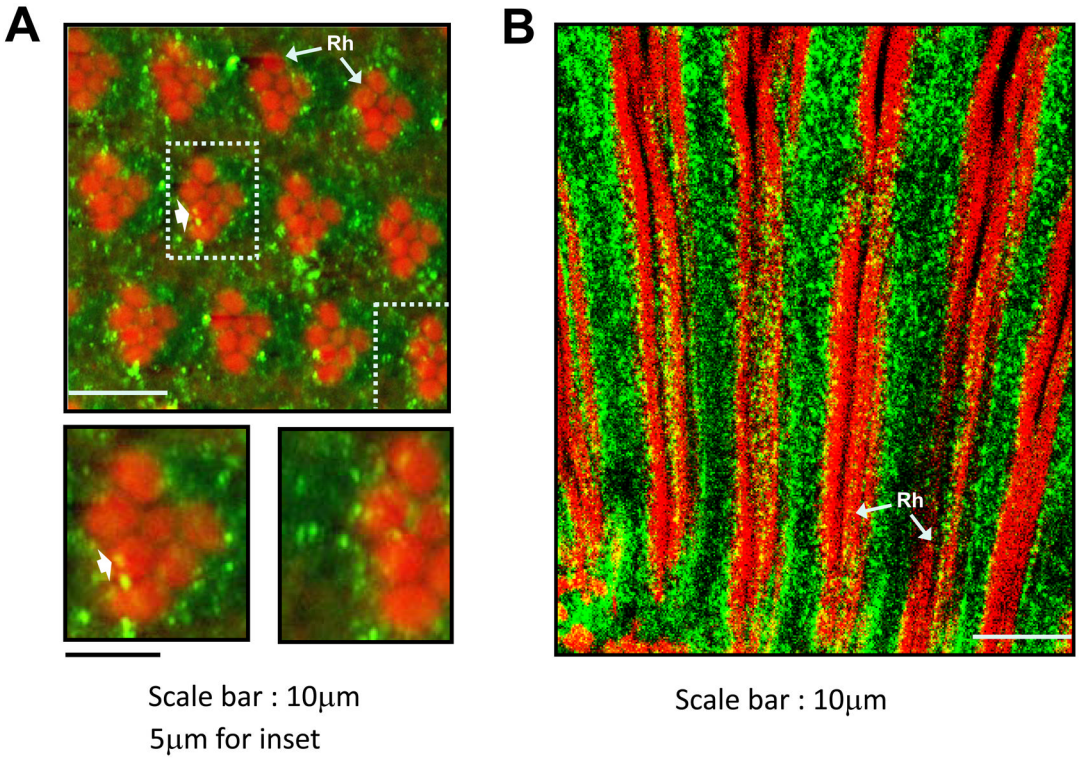

Fig. 5. Fluorescence confocal microscopy of the photoreceptor layer

A) A cross-sectional image taken ~35 μm from the distal tip of the ommatidia. Insets show the two highlighted ommatidia in higher magnification. Occasionally, some puncta are seen well inside the rhabdomres (arrow). **B)** A longitudinal section showing nearly the entire length of the ommatidia. Green: anti-INAE; red: F-actin in rhabodomeres. Rh: rhabdomere.

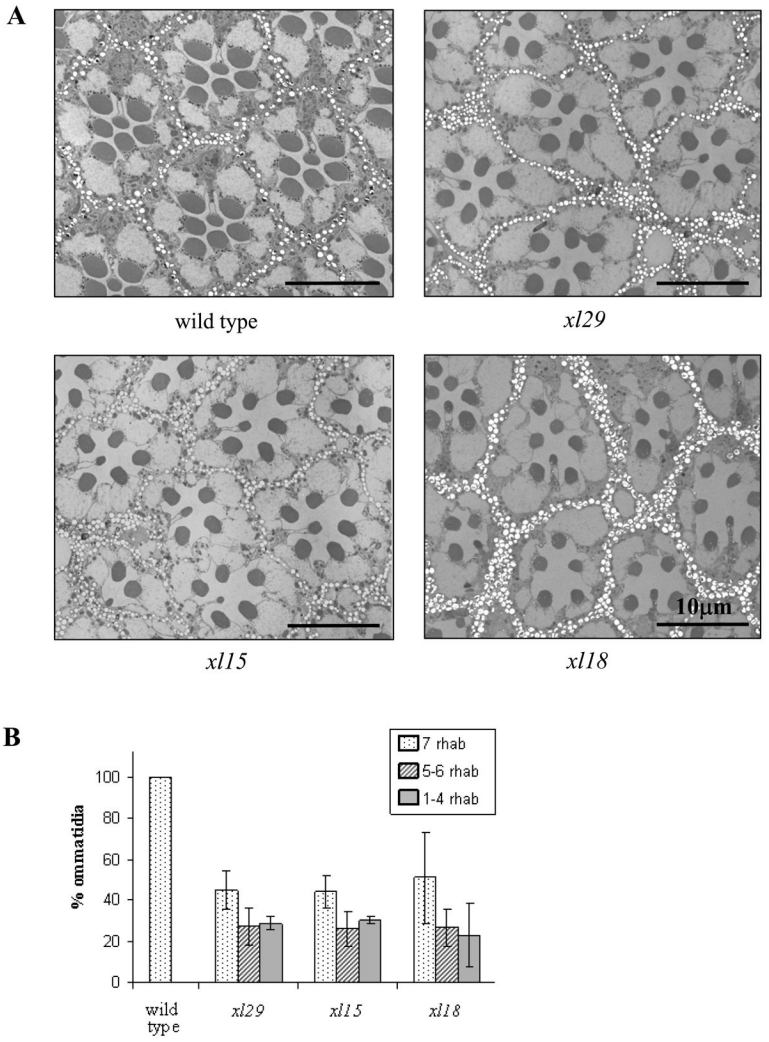

Fig. 6. Electron microscopy of *xl* ommatidia

A) Transverse sections of groups of ommatidia obtained at ~35 μm depth from the distal tips of rhabdomeres in 2–3 d post-eclosion wild type, *xl129*, *xl15* and *xl18*. **B)** Fractions of ommatidia containing 7, 5–6, and 1–4 rhabdomeres in wild type, *xl29*, *xl15* and *xl18*. The number of rhabdomeres in each ommatidium was counted in low magnification views of the entire section in 4, 4, 3, and 4 different eyes of wild type, *xl29*, *xl15*, and *xl18*, respectively.

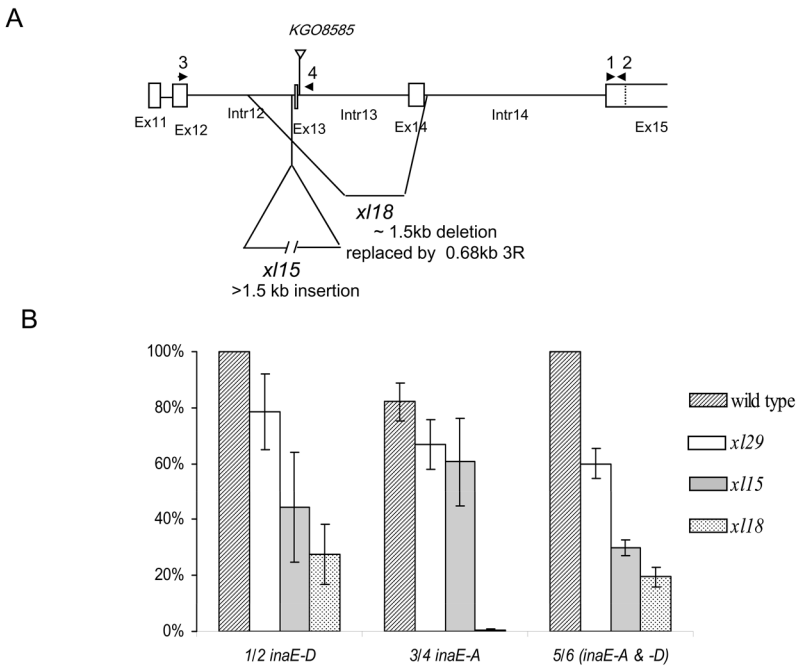

Fig. 7. A) Molecular alterations in *xl* mutants

xl29 had no mutation in the *inaE* gene, *xl15* carried a >1.5 kb insertion just upstream of Exon 13 (determined within 50 bp), and *xl18* carried a ~1.5 kb deletion, which was replaced by a 0.68 kb sequence translocated from the right arm of the third chromosome. **B)** Quantitative RT PCR measurements, based on three repetitions. All values obtained with primer pairs 1/2 and 3/4 were normalized with respect to those of *inaE-D* specific transcript of wild type. Those values obtained with the primer pair 5/6 were normalized with respect to wild type values within that series. No *inaE-A* transcript was detected in *xl18* because the A-form specific sequence was deleted in the mutant. Because the primer pair 5/6 amplified a much larger product than 1/2 or 3/4 (~400 bp vs. <150 bp), the amplification was less efficient. Locations of primer pairs 1/2 and 3/4 are shown in **(A)**. The primer pairs 5/6 were located in the 4th and 7th exons, respectively.

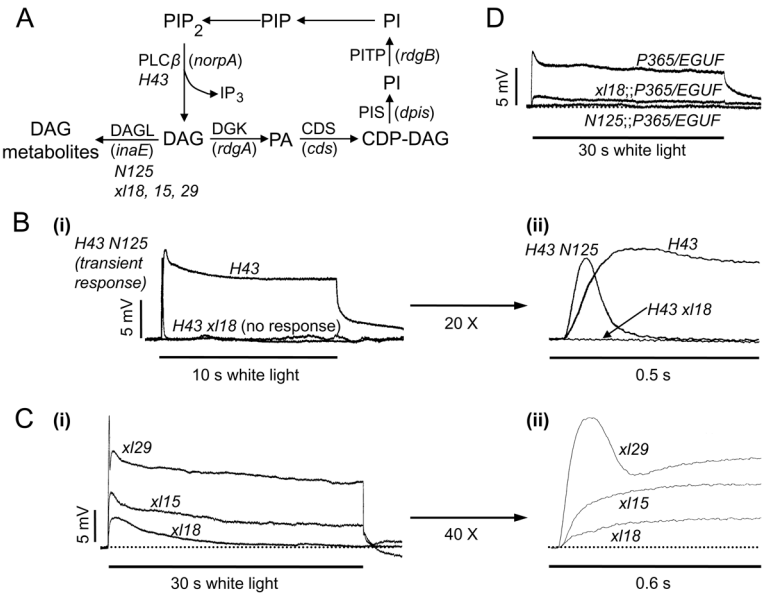

Fig. 8. Analyses of *inaE* mutants and double mutants

A) A diagram depicting a part of the phototransduction cascade and the phosphoinositide recycling pathway. Names of the genes encoding the proteins are shown in parentheses, and the mutants used in the present study are shown in italics under the protein names. *H43: norpA*^{H43}; *N125: inaE*^{N125}; *xl18: inaE*^{xl18}. **B)** *norpA inaE* double mutant study. **B-i)** Intracellular recordings of the receptor potentials elicited from the *H43* mutant are compared with those obtained from the *H43 N125* or *H43 xl18* double mutant. Receptor potentials of 12.5 ± 2.9 mV peak amplitude and 6.4 ± 2.3 mV steady-state amplitude were obtained from *H43* by a bright white stimulus of 10 s duration. The same stimulus elicited a fast transient response of 11.5 ± 2.4 mV peak amplitude with no steady-state component from the *H43 N125* double mutant and no response at all from the *H43 xl18* double mutant. **B-ii)** Initial portions of the responses shown in **B-i** are displayed in an expanded time scale. **C)** *inaE* mutations, *xl15*, *xl18* and *xl29*. **C-i)** Intracellular recordings of receptor potentials elicited by a bright, white, 30 s stimulus from *xl18*, *xl15*, and *xl29* are shown superimposed. **B-ii)** The initial portions of the responses in **C-i** are shown expanded in time scale by 40x. Quantification of the data, including those from *N125*, is presented in Table 2. **D)** Enhancement of the *P365/+* phenotype. Introducing *N125* to the *P365/+* background abolishes the small, ~7 mV receptor potential present in *P365/+*. Replacing *N125* with *xl18* makes the phenotype of the double mutant less severe. *EGUF* is wild type for *P365*. Because it is needed in *xl18;P365/EGUF* to make the fly mosaic for *xl18*, it was also introduced in other genotypes to maintain the same genetic background.

Table 1

Quantification of the data in Fig. 1.

Data summary of Fig. 1 B

	Peak amplitude (mV)	% Recovery of Peak amplitude at				
		10 s	30s	70 s	110 s	150 s	180 s
wt (n = 6)	28.8 ± 4.8	91 ± 4	103 ± 4				
N125 (n = 9)	24.7 ± 3.6	27 ± 11	55 ± 16	85 ± 11	93 ± 8	96 ± 4	
P343 (n = 6)	18.5 ± 3.9	2 ± 2	22 ± 14	78 ± 12	85 ± 17	95 ± 4	96 ± 4

Data summary of Fig. 1 C

genotype (mean peak amplitude ± S.D. in mV) (n = 7 for all except #) wt (28.2 ± 3.4); *P365*/+ (14.0 ± 2.3); *P365/P365* (0.5 ± 0.3); *N125;;P365*/+ (0.4 ± 0.3); *N125/P-line;;P365*/+ (3.0 ± 0.3); *P-line/P-line;;P365*/+ (4.8 ± 0.7); *N125;;P365*/*P*[*inaE-RD*] (14.4 ± 2.4); *N125;P*[*inaE-RA*];*P365*/+ (1.2 ± 0.6) (n = 5)#

Data summary of Fig. 1D

(n = 7 for all)	Peak amplitude (mV)	% peak amplitude at 30 s white light
wt	30.5 ± 1.5	56 ± 4
N125	26.8 ± 2.9	21 ± 7
N125;;P[*inaE-RD*]	30.9 ± 2.5	60 ± 4
N125;P[*inaE-RA*]	28.9 ± 2.9	13 ± 9

Table 2

Quantification of receptor potential parameter measurements.

Measurements were made on the following parameters of the receptor potential by intracellular recordings: peak amplitude, activation rate, latency, and amplitude at 30 s. The activation rate was defined as the slope of the straight line running from the initiation of the response to one-half peak amplitude. **A)** *inaE* mutants. The parameters obtained from *xl29* were indistinguishable from those of wild type. **B)** Enhancement of *P365/+*. The milder *inaE* mutation, *N125*, displayed conspicuously stronger enhancement of *P365/+* than *xl18*.

	Peak amplitude (mV)	Activation rate (mV/s)	Latency (ms)	Amplitude at 30s (mV)
***A. inaE* mutants**				
xl29 (n = 9)	20.4 ± 1.4	407 ± 58	12.9 ± 1.4	9.8 ± 1.3
N125 (n = 10)	*19.6* ± 2.7	219 ± 19	16.5 ± 1.3	3.0 ± 0.5
xl15 (n = 7)	8.6 ± 1.4	110 ± 17	16.3 ± 1.6	4.3 ± 0.8
xl18 (n = 8)	4.9 ± 0.5	53 ± 11	16.0 ± 1.0	0.5 ± 0.5
B. Enhancement of *P365*/+ (n = 7 for all)				
P365/EGUF	7.4 ± 2.4	77 ± 11	13.2 ± 1.2	4.0 ± 1.5
xl18;;P365/EGUF	1.2 ± 0.3[§]	*	16.2 ± 2.3	0.3 ± 0.2
N125;;P365/EGUF	0.2 ± 0.3[§]	*	*	*

*Too small to be determined accurately.

[§]The peak amplitude of *xl18;P365/EGUF* is significantly larger than that of *N125;P365/EGUF* ($P < 0.0001$).

Table 3

Quantification of resting potential measurements.

A) Resting potentials were determined from *inaE* mutants (*N125*, *xl15*, *xl18*), *norpA inaE* double mutants (*H43 N125*, *H43 xl18*), *rdgA* mutant (*P35*), and controls (wt, *xl29*). Resting potentials were normal in all genotypes except in *rdgA*. **B)** Interaction with *P365/+*. Introduction of *N125*, but not *xl18*, into the *P365/EGUF* background significantly depolarized the resting potential.

Resting potential (mV)			
A. *inaE* mutants, double mutants, *rdgB* mutant, and controls			
wt	−56 ± 6 (n = 7)	*N125*	−58 ± 3 (n = 7)
xl29	−55 ± 5 (n = 7)	*H43 xl18*	−51 ± 3 (n = 7)
xl15	−53 ± 5 (n = 7)	*H43 N125*	−55 ± 5 (n = 6)
xl18	−52 ± 4 (n = 8)	*P35*	−43 ± 5* (n = 8)
B. Interaction with *P365/+*			
P365/EGUF	−41 ± 3* (n = 7)		
xl18;;P365/EGUF	−41 ± 4* (n =7)		
N125;;P365/EGUF	−28 ± 3§ (n = 7)		

*Significantly smaller than the wild-type value ($P < 0.0002$);

§Significantly smaller than those marked with * ($P < 0.0001$).